CB Report 340

$\bar{p}p \to \pi^0\eta$ and $\pi^0\eta'$ from 600 to 1940 MeV/c

A.V. Sarantsev and D.V. Bugg

1 Introduction

Data on these channels were processed with identical procedures to $\pi^0\pi^0$, $\eta\eta$ and $\eta\eta'$. We therefore refer you to Technical Report 337 on $\bar{p}p \to \pi^0\pi^0$ for details of software which has been used and for $\pi^0\pi^0$ results. You will probably find it relevant to compare results with those of Technical Report 338 on the final states $\eta\eta$ and $\eta\eta'$.

We shall report results for $\pi^0\eta$ from both 4γ and 8γ events. The 4γ data for $\pi^0\eta$ are superior statistically by a factor 5 compared with 8γ, and have lower backgrounds. For $\pi^0\eta'$, the 4γ data are contaminated to an unacceptable level ($\sim 40\%$) by backgrounds from the prolific channels $\pi^0\pi^0\pi^0$ and $\omega\pi^0$, $\omega \to \pi^0\gamma$ after loss of two photons in the former case and one in the latter. Those backgrounds are predicted by the Monte Carlo simulation and we have been unable to find ways of removing them without unacceptable loss of events. So we deduce $\pi^0\eta'$ results purely from 8γ events where background are much lower. Numbers of events are listed in Table 1 after background subtractions described below.

2 Selection Criteria

The 4γ events have been selected, after kinematic fitting, with the following cuts on confidence level (CL): (i) $CL(\pi^0\pi^0) < 0.01\%$, (ii) $CL(\pi^0\eta)$ better than the remaining channels $\eta\eta$, $\eta\eta'$ and $\pi^0\eta'$, (iii) in the few cases where more than one combinatoric $\pi^0\eta$ solution is found, events are required to have CL at least a factor 10 better than the second solution, (iv) $CL(\pi^0\eta) > 10\%$. The $\eta \to \gamma\gamma$ signal is shown in Fig. 1(a) from events fitted kinematically to $\pi^0\gamma\gamma$ after cuts (i)–(iii). The very small background is compatible with the estimate of 1.3% from the Monte Carlo simulation. The sources of background at 1800 MeV/c are shown in Table 2, and those at other momenta are similar. Within errors, the background is isotropic and is subtracted under that assumption.

The confidence level distribution for events fitting $\eta\pi^0 \to 4\gamma$ after cuts is

Momentum (MeV/c)	$\pi^0\eta \to 4\gamma$	$\pi^0\eta \to 8\gamma$	$\pi^0\eta' \to 8\gamma$
1940	33960	3804	458
1800	34430	4786	531
1642	35551	5297	496
1525	32014	5102	504
1350	47176	7450	979
1200	72458	11622	1818
1050	51070	8027	1241
900	58739	10979	2126
600	12143	2493	627

Table 1
Numbers of events at each momentum.

Channel	Background(%)		
	$\pi^0\eta \to 4\gamma$	$\pi^0\eta \to 8\gamma$	$\pi^0\eta' \to 8\gamma$
$3\pi^0$	0.8	-	-
$\omega\pi^0$	0.2	-	-
$2\pi^0$	0.2	-	-
$\eta\pi^0\pi^0$	0.1	-	-
$4\pi^0$	-	2.6	2.6
$\eta\pi^0\pi^0\pi^0$	-	-	9.7
$5\pi^0$	-	-	1.6
$\omega 3\pi^0$	-	-	0.1
Total	1.3	2.6	14.1

Table 2
Estimated sources of background at 1800 MeV/c in $\pi^0\eta \to 4\gamma$ and 8γ, and $\pi^0\eta' \to 8\gamma$.

shown on Fig. 2(a) (full curve) and compared with the Monte Carlo simulation (dashed). There is good agreement down to 2% confidence level and we find that angular distributions and absolute normalisations are insensitive to exactly where the confidence level cut is set within the range 2–20%. Figs. 2(b) and (c) show corresponding results for $\pi^0\eta \to 8\gamma$ and $\pi^0\eta' \to 8\gamma$.

The $\pi^0\eta$ sample from 8γ data has been selected with the following confidence level cuts: (i) $CL(4\pi^0) > 10\%$, (ii) $CL(4\pi^0)$ better than other 4-body channels.

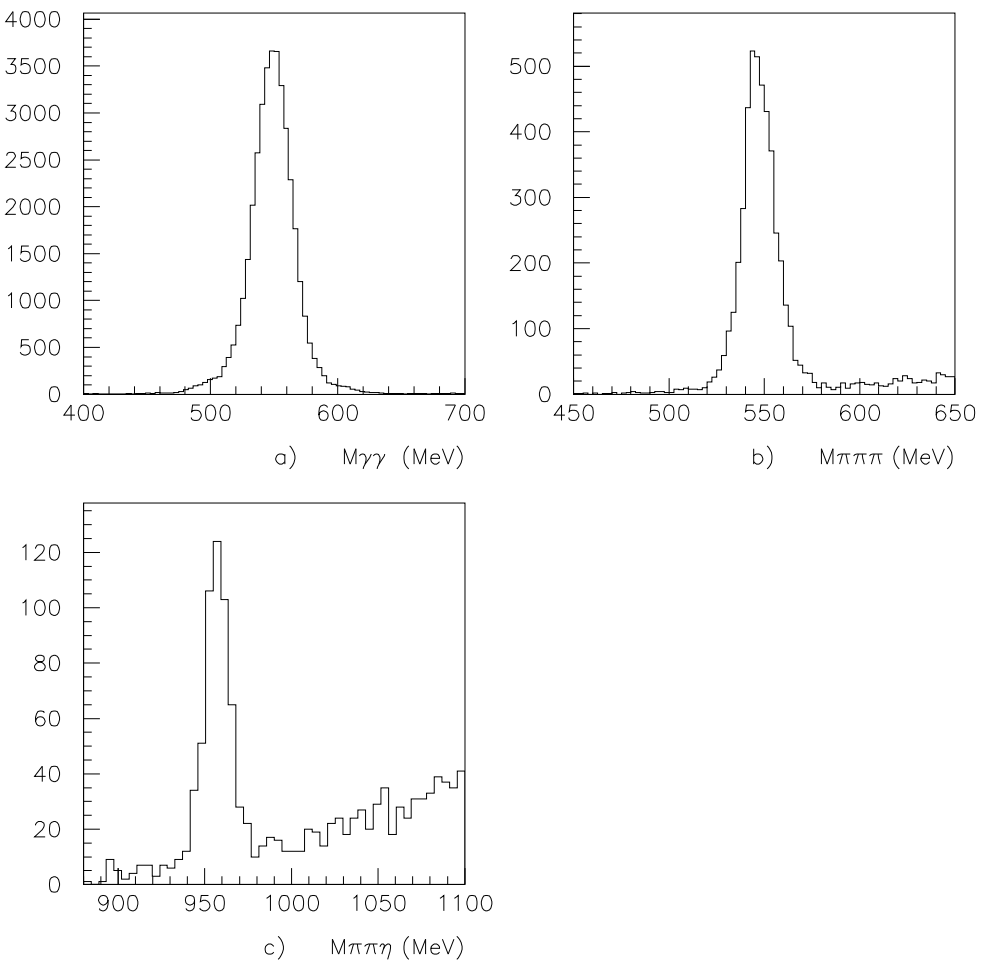

Fig. 1. (a) $M(\gamma\gamma)$ near the η from events fitting $\pi^0\gamma\gamma$, after cuts independent of the η. (b) $M(\pi^0\pi^0\pi^0)$ near the η from events fitting $4\pi^0$, after cuts independent of the η, (c) $M(\eta\pi^0\pi^0)$ near the η' from events fitting $\eta 3\pi^0$, after cuts independent of the η'. Data are at 1800 MeV/c.

(iii) any of the rare combinatoric alternatives has CL a factor 10 lower than that selected. The $\eta \to 3\pi^0$ signal from $4\pi^0$ events after these cuts is shown in Fig. 1(b). The background level of 3% is isotropic within errors and is marginally above the sources of background shown in Table 2 from the Monte Carlo simulation.

Results on $\bar{p}p \to \pi^0\eta'$ from 8γ events are selected with a 10% confidence level cut for $\eta\pi^0\pi^0\pi^0$. Further requirements are: (i) $CL(4\pi^0) < 0.01\%$, (ii)

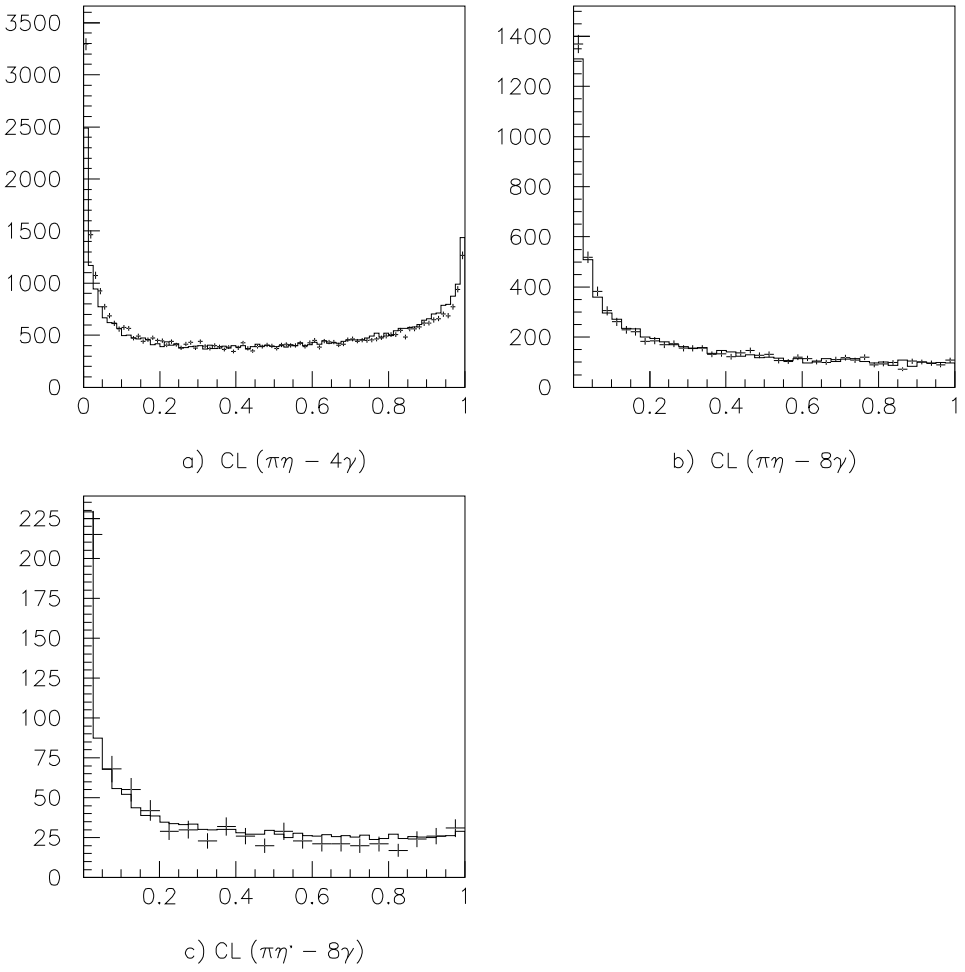

Fig. 2. Confidence level distributions for (a) $\pi^0\eta$ from 4γ data, after applying cuts to suppress backgrounds, (b) $\pi^0\eta$ from 8γ data after cuts and (c) $\pi^0\eta'$ from 8γ data after cuts. Full histograms show results from data and dashed histograms show Monte Carlo predictions.

$CL(\eta\pi^0\pi^0\pi^0)$ better than any other 8γ channel, (iii) $CL(\pi^0\eta')$ a factor 10 better than any combinatoric alternative. Fig. 1(c) shows the mass distribution from $\eta\pi^0\pi^0$ combinations after cuts. There is a clear η' peak, from which angular distributions are derived requiring $M^2(\eta\pi\pi)$ between 0.89 and 0.935 GeV^2. A side-band estimate of the background is made around the η' in the region shown and is isotropic within errors; it is subtracted with that assumption. The background level is typically 14%, in agreement with the the Monte Carlo simulation, which estimates the backgrounds shown earlier in Table 2.

3 Angular distributions and Normalisation

Angular distributions should be symmetric forward-backward in the centre of mass, because of limitations in the angular momentum states. Full histograms on Fig. 3 show data at several momenta on $\pi^0\eta$ from 4γ uncorrected for acceptance; dashed histograms show the acceptance. Fig. 4 shows angular distributions corrected for acceptance. Figs. 5 and 6 show corresponding results for $\pi^0\eta$ from 8γ events. The acceptance drops for forward $\eta \to 3\pi^0$ because of loss of photons down the beam pipe. Figs. 7 and 8 show corresponding results for $\pi^0\eta'$. In forming differential cross sections shown later, we have formed the weighted mean of results in forward and backward hemisphere, with a weight constructed from Poisson statistics for data and Monte Carlo. For 8γ events this weighting is obviously important.

You can make your own judgements whether or not angular distributions of Figs. 4,6 and 8 are really symmetic within statistics. At some momenta, there do seem to be slight and irregular asymmetries, but if so they vary from momentum to momentum. We are pretty sure that any such effects originate from the finite size of the crystals. The software tends to reconstruct showers near the centres of crystals, rather than uniformly across the faces of the crystals. We have illustrated this in the first Technical Report on Normalisation. Even if such an effect is present, it simply alters slightly the boundaries of bins of $\cos\theta$. There are 20 bins of $\cos\theta$ and we are fitting physics with angular distributions having Legendre Polynomials up to order 10. So this redistribution has no significant effect on physics conclusions, as we have demonstrated by an explicit numerical simulation. Remember, too, that the effect tends to get washed out by combining angular distributions from forward and backward hemispheres.

Fig. 9 shows the angular distributions for $\pi^0\eta$ final states from 4γ events (black triangles) and 8γ events (open circles). Both have been corrected for acceptance. There is excellent agreement, but the statistics on the latter are significantly poorer. The agreement is a satisfactory check on systematics. In particular we make one remark relevant to the questions concerning absolute normalisation. The rate dependence of the absolute normalisation is clearly visible for 8γ data at many momenta. It is unreasonable to believe that $\pi^0\eta$ events in 8γ should behave differently to other 8γ events. Indeed, we have been able to check that the signal/background ratio for the $\eta \to 3\pi^0$ signal does not change significantly with rate. Since $\pi^0\eta$ data agree between 4γ and 8γ, the inference is that the rate dependence must be present for 4γ data too.

The acceptance for 4γ data is shown by dotted curves on Fig. 9 It falls sharply at about $|\cos\theta| = 0.85$ and we discard data above $\cos\theta = 0.9$.

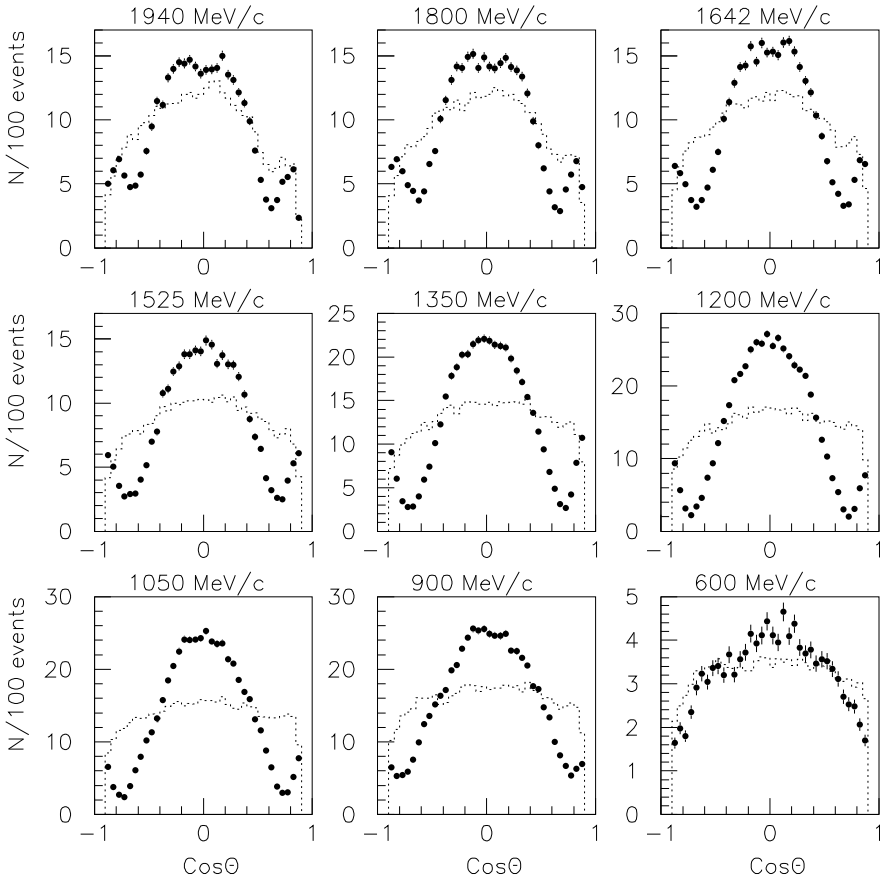

Fig. 3. Raw data $\pi^0\eta \to 4\gamma$ from both forward and backward hemispheres (full histogram) and the acceptance from Monte Carlo events (dashed).

Fig. 10 compares $\pi^0\eta$ data from 4γ with the earlier data of Dulude et al. [1] after adjusting their normalisation in order to secure the best agreement with ours. Data of Dulude et al are available at beam momenta of 1184, 1361, 1534, 1630, 1700 and 1957 MeV/c and are compared with the nearest of our beam momenta without any allowance for the slightly different momenta. There is fair agreement for the shape of the angular distributions, but some systematic disagreements.

Fig. 11 shows our cross sections integrated over the range $\cos\theta = 0$ to 0.85. Black triangles show 4γ data and open squares show 8γ data. There is good

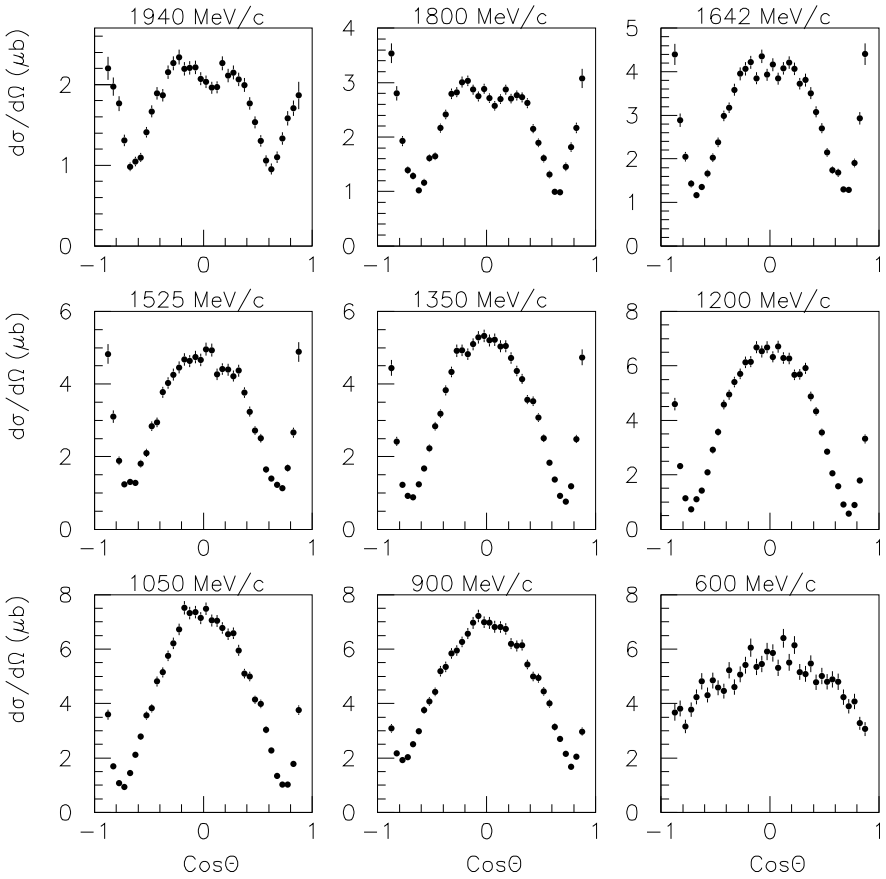

Fig. 4. Corrected angular distributions for $\pi^0\eta$ from 4γ events.

agreement. Open triangles show results of Dulude et al, integrated over the same angular range. They fall much lower than our data, as was the case for $\pi^0\pi^0$.

Angular distributions for $\pi^0\eta'$ are shown in Fig. 12 and are compared with fits described below. The integrated cross section form $\cos\theta = 0$ to 0.85 is showbn in Fig. 11(b), together with the fits.

Angular distributions have been fitted with Legendre polynomials. For $\pi^0\eta$, they require terms up to order 10 at the highest momenta. Because of the cut-off at $\cos\theta = 0.85$, there are large correlations between coefficients of the

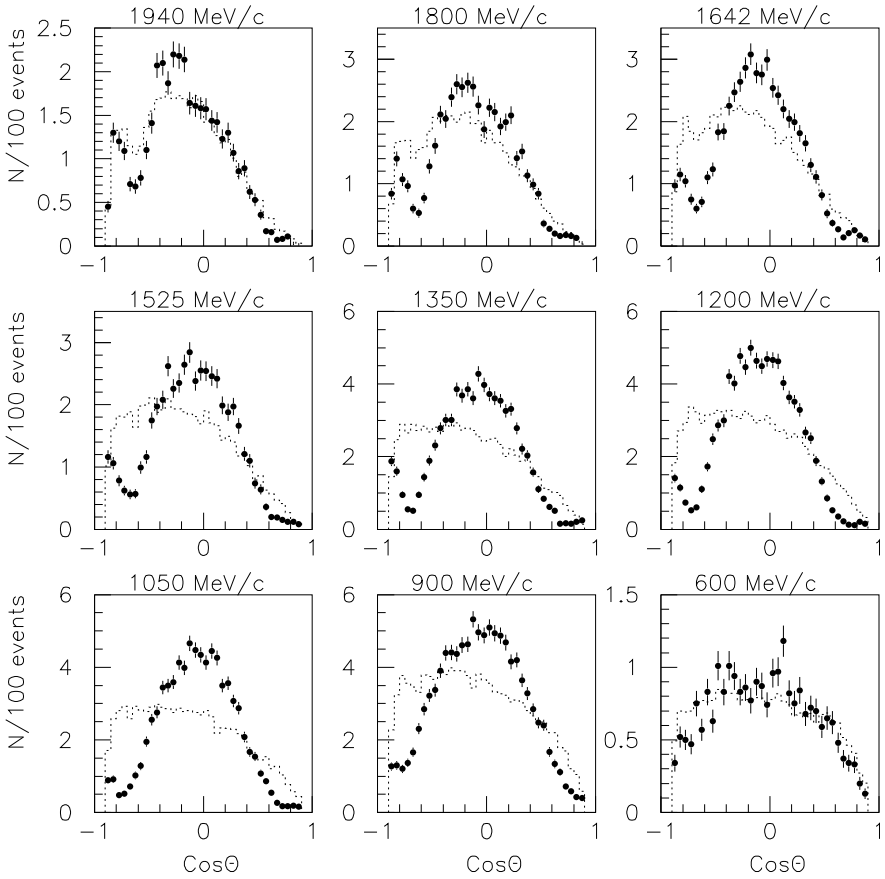

Fig. 5. As Fig. 3 for $\pi^0\eta$ from 8γ events.

Legendre series, and it is better to fit data directly.

4 Partial wave analysis

4.1 Introduction

From the quark model we expect two 0^+, four 2^+ and two 4^+ states in the mass region 1950-2350 MeV.

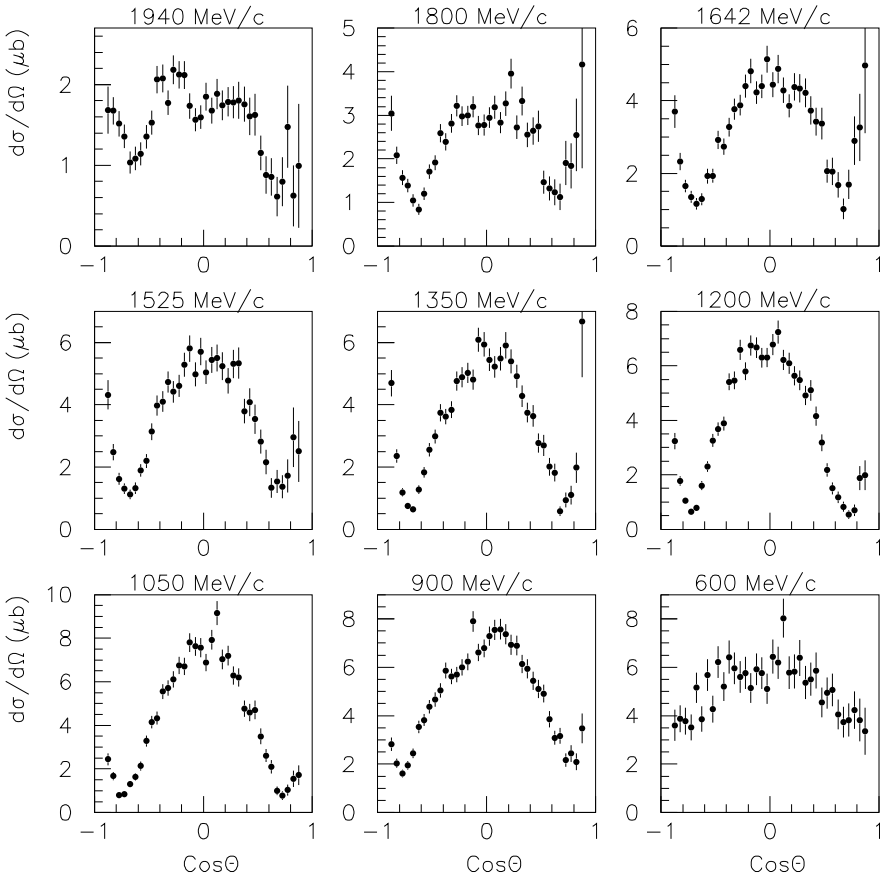

Fig. 6. As Fig. 4 for $\pi^0\eta$ from 8γ events.

First, the 0^+ state is expected to have mass 1980-2100 Mev and therefore to be a partner of either the $f_0(2020)$ resonance found by the Omega group or $f_0(2100)$ observed in $\eta\eta$ decay. The next 0^+ radial excitation should be located ~ 250 Mev higher, towards the top of the investigated region.

The 2^+ resonances can be either $^3P_2$ or $^3F_2$ $q\bar{q}$ states. The quark model calculations predict that $n = 3$ $^3P_2$ states have a mass in the region 1950-2050 MeV while the first $^3F_2$ state has a mass 40-80 MeV larger and thus located in the 2000-2100 mass region. The next radial excitations are expected to appear near 2300 MeV and there is a good possibility to find them in our analysis.

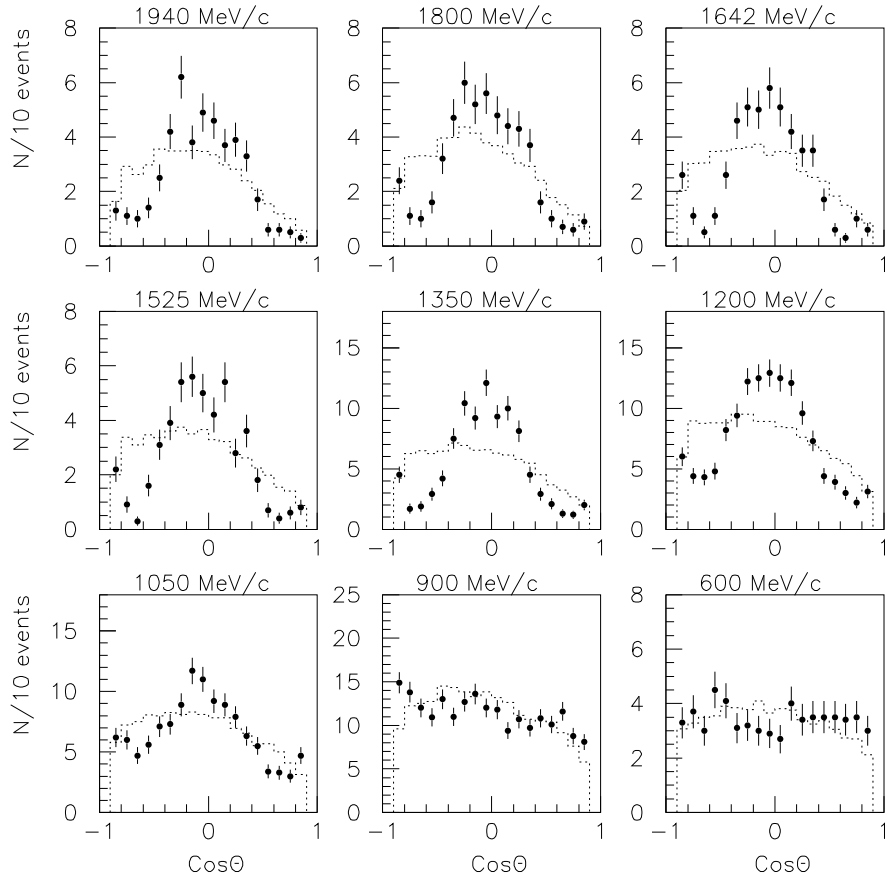

Fig. 7. As Fig. 3 for $\pi^0\eta'$ from 8γ events.

The 4^+ states must be ${}^3F_4$ $q\bar{q}$-states and located near ${}^3F_2$ states.

It would be probably rather difficult to observe the contribution of the states located above the available region, with the exception of the 6^+ state which is expected near 2500 MeV. The GAMS group has rather good evidence for an $f_6(2510)$ [2]. It provides the highest order of Legendre polynomial to the amplitude near the high energy boundary.

Another rather strong restriction for the data analysis is provided by $SU(3)$ relations for resonance decays into $\pi\eta$ and $\pi\eta'$ channels. The production coupling of a resonance can have an imaginary part due to possible coupling to the

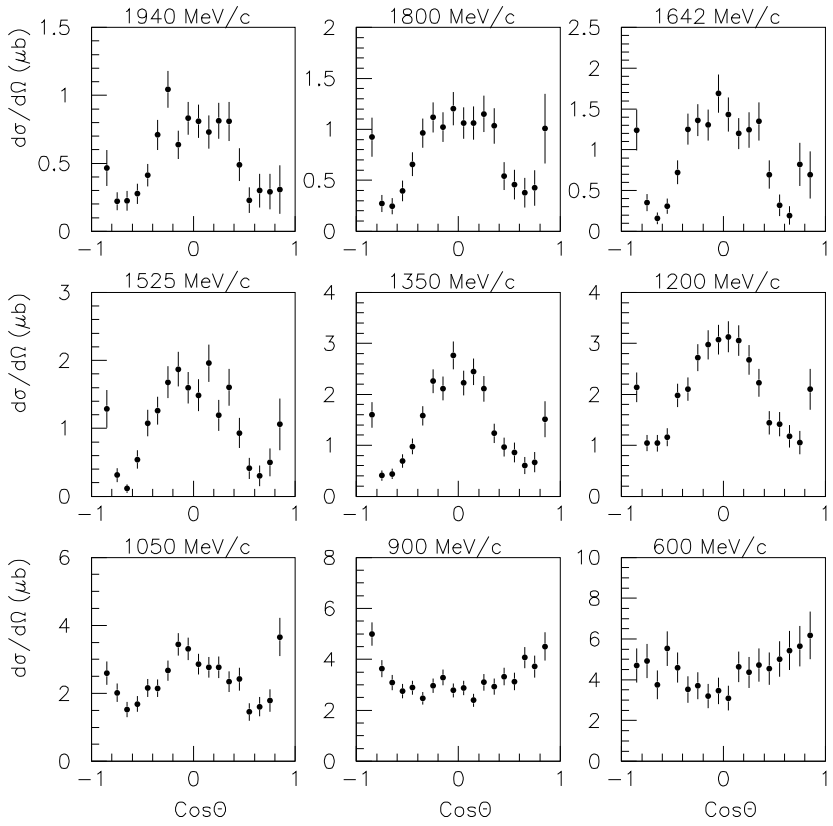

Fig. 8. As Fig. 4 for $\pi^0\eta'$ from 8γ events.

$p\bar{p}$ system via intermediate multi-meson states. However the relative phase of $\pi\eta$ and $\pi\eta'$ channels must be equal to zero unless there is a strong interference between resonances. In the case of decay of $q\bar{q}$ states, this amplitude ratio of $\pi^0\eta$ compared with $\pi^0\eta'$ is equal to the ratio R of nonstrange components in η and η' mesons, $R = 0.8/0.6$.

If there is no exotic state in the region, the meson-meson channels can only mix different radial excitations of states with the same quantum numbers. Usually such states are well separated in mass scale and we do not expect large mixing and therefore deviation of the relative $\pi\eta$-$\pi\eta'$ phase from zero.

Data may be fitted with any of the known approaches for data analysis. As soon as interference terms are small, T-matrix, K-matrix or N/D approaches

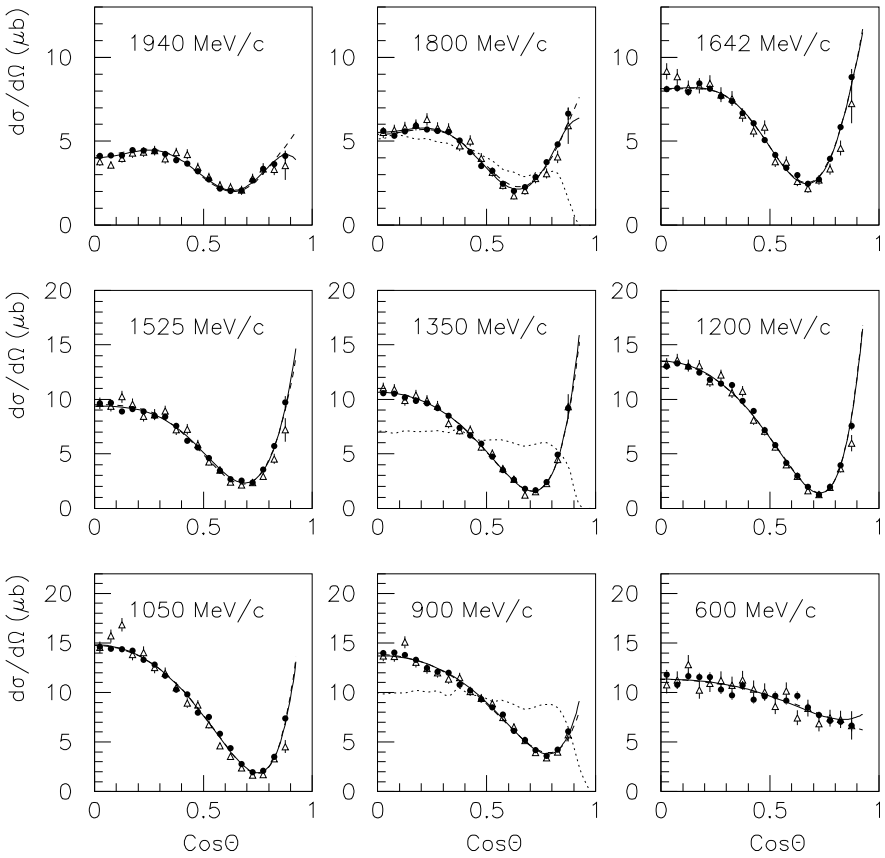

Fig. 9. Comparison of angular distributions for $\pi^0\eta$ from 4γ events (black circles) and 8γ (open triangles). Dotted curves illustrate the acceptance.

can be algebraically rewritten one in terms of another. A problem only appears when there are either presence of exotic states or large t-channel exchanges or large threshold effects. We expect such problems in isoscalar channels but in the isovector sector the situation should be quite simple.

Therefore one of our main objectives is to fit data as close as possible to SU(3) constraints, so as to define genuine $q\bar{q}$ states. Such information will be important for the detection of the exotic states in the isoscalar sector.

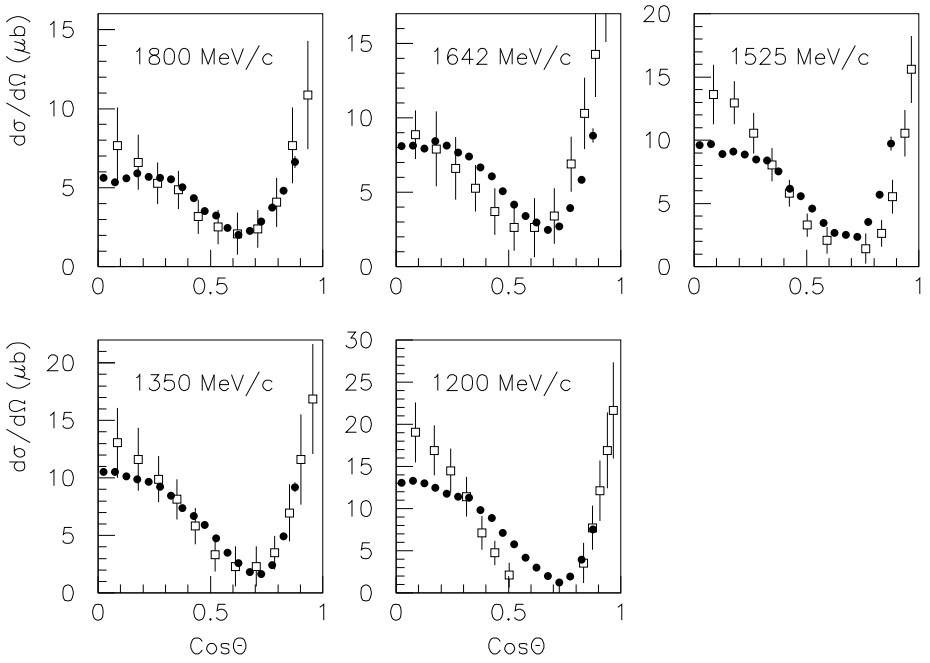

Fig. 10. Comparison of angular distributions for $\pi^0\eta$ from 4γ events (black circles) and the data of Dulude et al. (open squares).

4.2 Formulae

Formulae for differential cross sections in terms of partial waves have been given by Hasan and Bugg [3] and are repeated in CB report 337 on $\bar{p}p \to \pi^0\pi^0$. We fit the data in terms of a sum of s-channel resonances. Even if t-channel exchanges are present, partial wave amplitudes will acquire a phase variation from these resonance by Watson's theorem. That is, the amplitudes must share the Breit-Wigner denominator.

The T-matrix for each partial wave is parametrised as:

$$T_{L,J} = \sum_i \frac{G_i B_L(p) B_J(q)}{s - M_i^2 - i M_i \Gamma_i}, \tag{1}$$

where G_i are complex coupling constants, $B_L(p)$ is the standard Blatt-Weisskopf centrifugal barrier in terms of the momentum p in the $\bar{p}p$ channel, and $B_J(q)$ is the centrifugal barrier in terms of the momentum q in the $\pi\pi$ channel. This

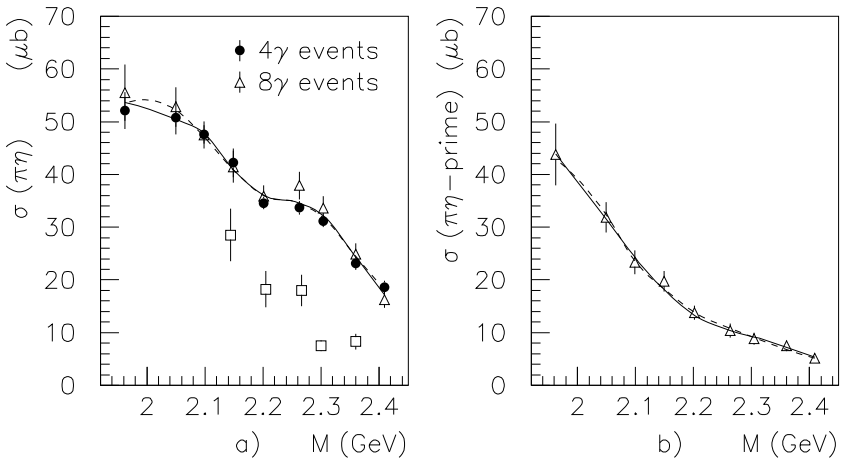

Fig. 11. Comparison of our cross sections integrated over the range $\cos\theta = 0$ to 0.85 for $\pi^0\eta$ from (a) 4γ events (black triangles) and 8γ (open triangles), (b) $\pi^0\eta'$. Results of Dulude et al for $\pi^0\eta$, integrated over the same angular range are shown by open squares.

parametrisation imposes the important constraint of analyticity. Unitarity is irrelevant, since the amplitudes are far below the unitarity limit, and we know nothing about the coupling to many channels.

4.3 Features of the fits

Our initial fits, first to $\pi^0\eta$ alone, then in combination with $\pi^0\eta'$, immediately demonstrated the need for one 0^+ resonance around 2000 MeV, two 2^+ resonances around 2050 and 2300 MeV and two 4^+ resonances around 2050-2100 MeV and near 2270 MeV. This confirmed the expected picture. Two solutions were found, as for $I = 0$. These solutions had closely similar masses and widths for resonances, and differences were mostly in coupling constants and phases.

It was immediately apparent that the amplitudes for 0^+ and 4^+ resonances were close to the SU(3) relation for coupling constants; furthermore, relative phases between $\pi^0\eta$ and $\pi^0\eta'$ were close to zero within errors of about 10°, as expected. Nevertheless, for spin 2 resonances, there was a large breaking of SU(3). Coupling constants came out with opposite signs; relative phases were well away from zero. Any attempt to enforce the SU(3) relations, even

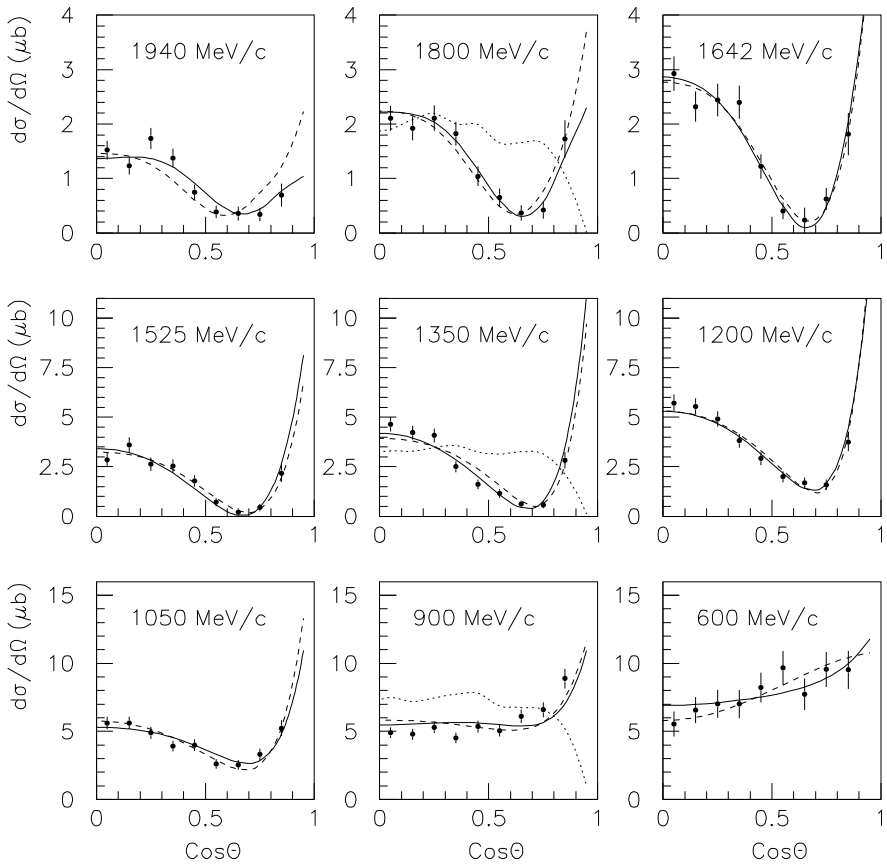

Fig. 12. Angular distributions for $\pi^0\eta'$ compared with the partial wave fits. The full curevs show solution 1 and the dashed curevs solution 2. Dotted curves illustrate the acceptance.

approximately, led to large increases in χ^2 of order 250–300. The discrepanccy was obviously largest for the 2^+ resonance near 2050 MeV.

In view of our general expectation that there could be four 2^+ states over this mass range, our next step was to add a third 2^+ resonance. This immediately solved the problem with SU(3), via interferences between a new 2^+ state just below 2000 MeV and the second one near 2050 MeV. The lowest state was dominantly $^3P_2$. The next required a significant $^3F_2$ component, though χ^2 does not change too much as the ratio of $^3P_2$ and $^3F_2$ amplitudes varies around

1:1. The highest 2^+ state optimises as dominantly ${}^3F_2$ in solution 1 and as dominantly ${}^3P_2$ in solution 2.

The fit does not like to obey the SU(3) relations exactly. A glance at the differential cross sections and integrated cross sections convinces one that the raw data deviate significantly from the SU(3) relation that $d\sigma/d\Omega(\pi^0\eta') = 0.5625 \times d\sigma/d\Omega(\pi^0\eta)$. So there must be a significant violation of SU(3) somewhere. It was immediately obvious that relative phases can be fixed at zero with almost no penalty in χ^2. However, the magnitudes of coupling constants for 4^+ and 2^+ reonances tend to drift lower for $\pi^0\eta'$ than the SU(3) relation. For 4^+ amplitudes, the ratios of $\pi^0\eta'$ and $\pi^0\eta$ coupling constants optimises freely at around 0.7 of the SU(3) value. For 2^+ it optimises in the range 0.8–0.85$\times$ the SU(3) value. For 0^+ it optimises 10% above the SU(3) value.

This pattern appears to us very reasonable. There is less phase space for $\pi^0\eta'$ than for $\pi^0\eta$. For 4^+ states, where there is a strong centrifugal barrier, one would expect the coupling constant for $\pi^0\eta'$ to fit somewhat below the SU(3) value, as observed. It is difficult to predict the magnitude of this effect, since it is very sensitive to the radius of the barrier. For 2^+ states, the coupling constants are closer to the SU(3) relation, as expected. For 0^+, the SU(3) relation can be satsified exactly if one introduces a small constant background amplitude.

4.4 Testing the fits

At this stage, we made an extensive search for alternative solutions. This was done in several ways. Phases of each resonance were changed in 90° steps and the solution was restarted. Coupling constants of pairs of 2^+ resonance were changed in sign; likewise for 4^+; also pairs of 2^+ and 4^+ resonances were treated in the same way. When solution 2 was perturbed, it frequently collapsed to solution 1. Otherwise, it converged to one of a family of local minima where fitted amplitudes, hence intensities, all look similar. It is clear that they are minor variants of one another. With some prodding, all can be induced to collapse to a single minimum.

Finally, masses and widths of resonances were stepped through a large range and all other parameters were re-optimised. At the first step of this re-optimisation, χ^2 increased by 2 or 3 orders of magnitude. Nevertheless, the solutions generally converged stably in 20–30 iterations, without encountering the local minima. This is a rather severe test of the stability of the solutions.

Incidentally, one fit takes typically 15-20 seconds fitting all data, so thousands of fits have been made.

4.5 Fitted Resonances

Table 3 shows the masses and widths of resonances fitted to solutions 1 and 2. The errors cover (i) 3σ increases in χ^2, (ii) the range of systematic variations observed amongst local minima for solution 2, and (iii) variations of the radius of the centrifugal barrier over the range 0.6–1.0 fm.

J^P	M (MeV/c^2)	Γ (MeV/c^2)	M (MeV/c^2)	Γ (MeV/c^2)
0^+	2026 ± 28	330 ± 75	1982^{+12}_{-80}	224^{+120}_{-32}
2^+	1992^{+15}_{-30}	190 ± 50	1975 ± 17	195^{+50}_{-80}
2^+	2060 ± 18	195 ± 29	2095^{+13}_{-21}	157 ± 28
2^+	2265 ± 20	235^{+60}_{-35}	2278 ± 13	295 ± 44
4^+	2025 ± 40	250^{+80}_{-50}	2130 ± 50	230 ± 80
4^+	2300 ± 16	230 ± 37	2265^{+67}_{-23}	275 ± 32

Table 3
Masses and widths of fitted resonances; columns 2 and 3 show solution 1 and columns 4 and 5 solution 2.

Intensities of all partial waves are shown in Fig. 13. Column 1 shows $\pi^0\eta$ for solution 1 and column 2 $\pi^0\eta'$; columns 3 and 4 show corresponding results for solution 2. The dashed curves show results for $^3P_2$ and $^3F_4$; dotted curves show results for $^3F_2$ and $^3H_4$. Interferences disappear in the sum, which is shown by the full curves. The 4^+ amplitudes in both solutions are almost purely $^3F_4$ for the lower 4^+ resonance. One expects the $L = 5$ centrifugal barrier to inhibit coupling to $\bar{p}p$ $^3H_4$. The 6^+ amplitude is therefore restricted to $^3H_6$. It has fairly small effects on χ^2: 50 in solution 1 and 19 in solution 2. It has almost no effect on fitted masses and widths for other resonances. It is fitted with a mass of 2500 MeV and a width of 250 MeV. These are educated guesses, close to the GAMS values for $f_6(2510)$, the better established of the 6^+ resonances listed by the PDG.

We have fitted 405 $d\sigma/d\Omega$ points. Each angular distribution is allowed a normalisation constant with errors of $\pm 6\%$ at 600 and 900 MeV/c and $\pm 3\%$ at higher momenta (except 1940 MeV/c, where it is increased to $\pm 10\%$). These values are taken from the errors reported in the Technical Report on Normalisation. There are 37 parameters for resonance masses, widths, phases and coupling constants. For solution 1, $\chi^2 = 530$; for solution 2, it is significantly higher: $\chi^2 = 631$.

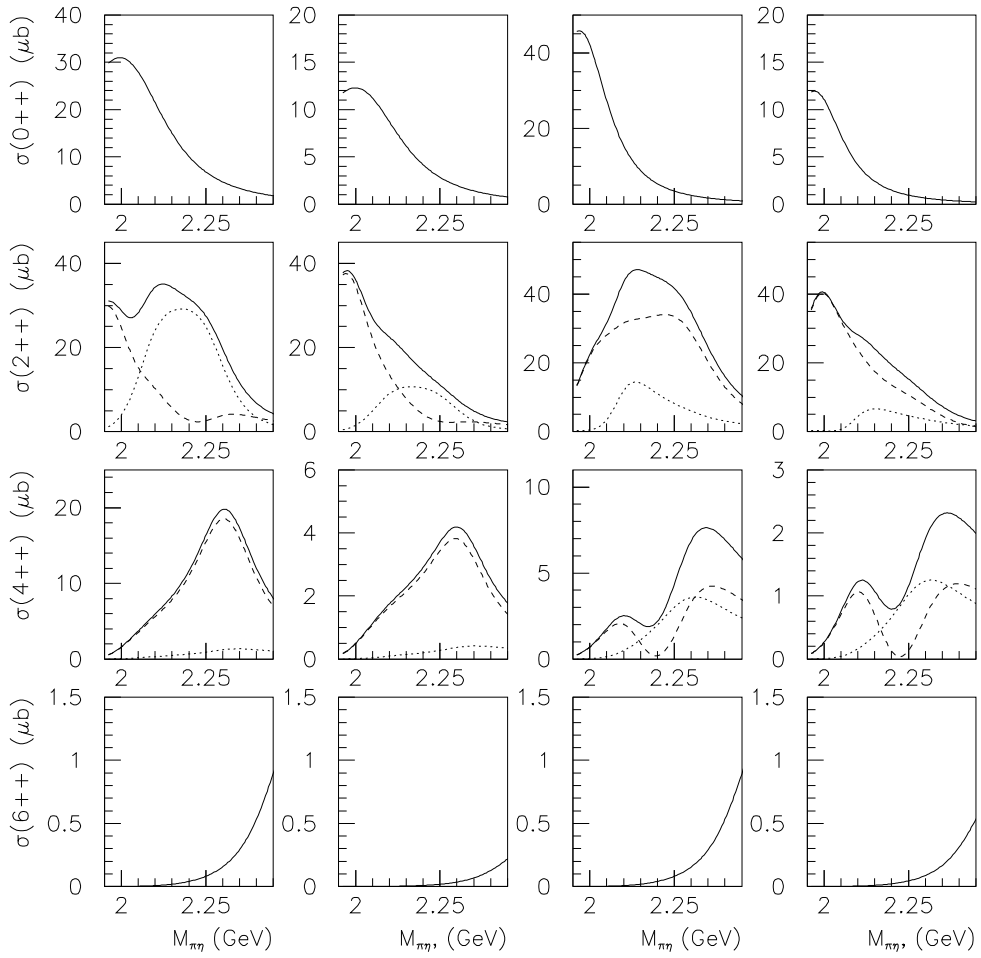

Fig. 13. Intensities fitted to $\pi^0\eta$ and $\pi^0\eta'$: solution 1 $\pi^0\eta$ column 1, $\pi^0\eta'$ column 2; solution 2 $\pi^0\eta$ column 3, $\pi^0\eta'$ column 4. Dashed curves show $^3P_2$ and $^3F_4$, dotted curves $^3F_2$ and $^3H_4$. Full lines show their sum.

This difference in χ^2 is one reason for preferring solution 1. The existence of local minima close to solution 2 suggests it is not too well defined. It requires the lower 4^+ resonance to have a mass of 2130 MeV; that is well above the expected mass of $\sim$ 2045 MeV for the partner of $f_4(2050)$. Privately, the VES and E852 collaborations have told us they have strong evidence for an a_4 in the mass range 1980–2010 MeV. Our value of 2025 ± 38 MeV for solution 1 looks a plausible compromise. The error is fairly large because of uncertainty in the effect of the centrifugal barrier.

There is one external piece of information favouring solution 1. We have completed fitting $3\pi^0$ data, and are in process of writing the draft paper and Technical Report. In these data, the upper 4^+ resonance is very conspicuous. It couples dominantly to ${}^3F_4$ with an intensity in ${}^3H_4$ which is about 30% of ${}^3F_4$. It looks remarkably similar to solution 1 and quite different to solution 2. For all these reasons, we anticipate that solution 1 is the correct one. Eventually we plan to make a combined fit to present data and $3\pi^0$ to test this conclusion.

Table 4 shows changes in χ^2 when each resonance is dropped from the fit and all remaining masses, widths and coupling constants are re-optimised. In all cases, χ^2 increases by over 100, so all these resonances are definitely required. We have tried adding a further 0^+ resonance around 2300 MeV. It does improve χ^2 by nearly 50 for both solutions, but there is no well defined optimum for its mass and width, so we omit it. We have tried introducing a constant 0^+ background, but it has little effect. Likewise, we have explored the possibilty of adding a fourth 2^+ resonance, but the fit becomes ill-defined.

Resonance	Solution 1	Solution 2
$f_4(2025-2130)$	206	232
$f_4(2301-2265)$	224	202
$f_2(1992-1975)$	494	386
$f_2(2060-2095)$	290	312
$f_2(2265-2278)$	228	388
$f_0(2026-1982)$	144	288
$a_6(2500)$	50	19

Table 4
Changes in χ^2 when each resonance is omitted and the remainding resonances and coupling constants are re-optimised.

5 Interpretation

The 2^+ resonance at or close to 2060 MeV is 60% ${}^3F_2$ in solution 1 and 90% in solution 2. we suggest it is the $\bar{q}q$ ${}^3F_2$ state expected at roughly this mass. It makes a partner for the $f_2(2020)$ we have observed in $I=0$ data on $\pi^0\pi^0$, $\eta\eta$ and $\eta\pi^0\pi^0$. It is close in mass to the well known $f_4(2050)$ which is generally assumed to be $\bar{q}q$ ${}^3F_4$. That identification makes the $a_2(1992-1975)$ a clear candidate for $\bar{q}q$ ${}^3P_2$; its dominant coupling to $\bar{p}p$ ${}^3P_2$ supports this interpretation. It is presumably the partner of $f_2(1920)$. Incidentally, the latest

VES data, as yet unpublished, move the mass of the f_2 up to 1938 MeV, with a width of 170 ± 20 MeV.

Around 2250–2300 MeV one expects Regge recurrences for both $^3P_2$ and $^3F_2$. There could easily be two resonance in this mass region, as yet unresolved. We hope a combined analysis with $3\pi^0$ data will resolve this ambiguity. Solution 1 favours $^3F_2$.

6 Summary

Both solutions 1 and 2 require two 4^+ resonance, at least two 2^+ resonance and one 0^+. If SU(3) is to be obeyed approximately, three 2^+ resonances are required, as in Table 3. Masses and widths of resonances are similar in the two solutions, which differ mostly in coupling constants and phases. Solution 1 has significantly better χ^2. It has a better defined minimum, a more likely mass for the 4^+ resonance close to $f_4(2050)$ and is closely consistent with $3\pi^0$ data.

References

[1] R.S. Dulude et al., Phys. Lett. 79B (1978) 329.

[2] Particle Data Group, Euro. Phys. J. 3(1998) 1.

[3] A. Hasan and D.V. Bugg, Phys. Lett. B334 (1994) 215.